J. Fluid Mech. (2000), *vol.* 422, *pp.* 225–248. Printed in the United Kingdom

Dynamics of cooling domes of viscoplastic fluid

By N. J. BALMFORTH[1] AND R. V. CRASTER[2]

[1]Department of Applied Mathematics and Statistics, School of Engineering, University of California at Santa Cruz, CA 95064, USA

[2]Department of Mathematics, Imperial College of Science, Technology and Medicine, London, SW7 2BZ, UK

(Received 10 December 1999)

A non-isothermal viscoplastic thin-layer theory is developed to explore the effects of surface cooling, yield stress, and shear thinning on the evolution of non-isothermal domes of lava and laboratory fluids. The fluid is modelled using the Herschel–Bulkley constitutive relations, but modified to have temperature-dependent viscosity and yield stress. The thin-layer equations are solved numerically to furnish models of expanding, axisymmetrical domes. Linear stability theory reveals the possibility of non-axisymmetrical, fingering-like instability in these domes. Finally, the relevance to lava and experiments is discussed.

1. Introduction

This article explores the dynamics of a cooling viscoplastic fluid which is extruded onto a horizontal plate and spreads under gravity. The study is theoretical and motivated by a particular problem in geological fluid mechanics: the expansion of silicic lava domes. We continue a previous article (Balmforth *et al.* 1999, referred to herein as paper I) that dealt with isothermal viscoplastic fluids.

Lava domes are created when crystal-rich silicic magma emerges from a vent and take a variety of forms depending upon the effusion rate and magma rheology (Blake 1990; Fink & Griffiths 1998). Despite their low aspect ratio and slow evolution, these structures are challenging objects to model because of their composition: silicic lava is a strongly non-Newtonian fluid, with a significant yield stress and highly temperature-dependent material properties (McBirney & Murase 1984). The fluid rheology is complicated yet further by the phase change of solidification. These complications have placed an effective barrier to mathematical discussions of the problem, and earlier theoretical work is mostly confined to dimensional scaling arguments (see Griffiths & Fink 1993). However, a mathematical approach is not the only avenue open.

Several previous studies of lava domes have chosen a more practical route and conducted laboratory experiments with analogue fluids. Here, the lava is represented by a fluid with similar and (apparently) known rheological properties. Experiments then allow one to study dome evolution in a controlled environment. In this way, isothermal lava domes have been modelled using viscous fluids (Huppert *et al.* 1982) and water–kaolin slurries (Blake 1990); viscous fluids have no special significance for lava, but clay slurries possess a yield stress. Analogue laboratory models of non-isothermal domes have been developed using wax and corn syrup, fluids with

temperature-dependent material properties (Fink & Griffiths 1992; Stasiuk, Jaupart & Sparks 1993).

To date, the most ambitious analogue modelling has been conducted by Griffiths & Fink (1997), who used a mixture of Polyethylene Glycol wax and kaolin. This slurry has both a yield stress, a temperature-dependent viscosity, and solidifies near typical room temperatures. Hence, this analogue material possesses three of the most significant non-Newtonian effects present in lava. Griffiths & Fink's experiments provide a wealth of data to compare with theoretical models. The experiments have also been successful in rationalizing morphology seen in real lava flows: expanding domes of clay–wax slurry can lose axisymmetry and develop complex non-axisymmetrical shapes resembling 'lobes' or 'petals'; similar features are also seen in real lava domes.

Our purpose in this article is to continue to develop a mathematical model of both lava domes and experimental extrusions. We aim to model both because the slurry domes are more accessible, and through understanding their dynamics we can identify which features may also carry over to lava. The goal is to construct a model that captures the important physics of lava domes and reproduces their structure and evolution. However, this is a challenging enterprise both for the reasons mentioned above, and because of further mathematical problems that are uncovered in the present analysis. For this reason, we narrow our focus here and consider an idealized problem: the expansion of a cooling viscoplastic fluid in the absence of solidification. We do this both in the interests of simplicity, and because we would first like to understand the dynamics of purely fluid domes.

Our study consists of four major parts. First, we summarize the essential physics. This is the content of the next section. Then, by a suitable non-dimensionalization (see § 3) we isolate the important dimensionless parameters of the problem and set up the equations for asymptotic analysis. The parameterization should also aid experimentalists in selecting the most relevant analogue materials.

Second, we exploit a certain asymptotic limit to simplify the governing equations and derive a *thin-layer model* that can be used to study dome dynamics (§ 4). In this special limit, the dome has low aspect ratio, evolves slowly, and thermal diffusion acts sufficiently quickly to make the fluid isothermal in vertical cross-sections. Related thin-layer models have been used to study thermocapillary effects on spreading viscous drops (Ehrhard & Davis 1991) and spreading viscous melts in nuclear reactors (King, Riley & Sansom 2000). A similar rapid diffusion limit is also useful for Marangoni-driven thin-layer flows with a soluble surfactant (Jensen & Grotberg 1993). In § 5 we provide numerical solutions for axisymmetric, cooling domes, and indicate how thermal effects influence the dynamics in these models.

Third, we consider the development of non-axisymmetrical domes as a problem of pattern formation: one explanation for the appearance of lobes is that axisymmetrical expansion is linearly unstable to non-axisymmetrical perturbations. Indeed, analogies with other problems (notably Saffman–Taylor fingering, the Mullins–Sekerka instability in directional solidification, and thermocapillary droplet spreading – Patterson 1981; Ehrhard 1993) suggests that the interplay between surface cooling and temperature-dependent viscosity may give rise to thermal instabilities (see also Whitehead & Helfrich 1991). In § 6, we use the thin-layer model to study fingering-type instabilities and examine whether these can explain Griffiths & Fink's observations of slurry and lava morphology.

Finally, we discuss the relevance of the thin-layer model to real lava domes and analogue experiments. For lava, the dome is unlikely to be vertically isothermal because the diffusivity is small. Instead, the cooling of the surface creates a thermal

boundary layer that slowly migrates into the fluid interior. Nonetheless, the theory does appear relevant to some experimental materials.

2. Formulation

We consider a thin film of incompressible, non-isothermal fluid on a flat plane. In cylindrical polar coordinates (r, θ, z) the fluid is described by the velocity field, (u, v, w), density, ρ, pressure, p, and temperature, T. The equations for the film are given by conservation of momentum, mass and energy:

$$\rho\left(u_t + uu_r + \frac{v}{r}u_\theta + wu_z - \frac{v^2}{r}\right) = -p_r + \partial_r\tau_{rr} + \frac{1}{r}\partial_\theta\tau_{r\theta} + \partial_z\tau_{rz} + \frac{1}{r}(\tau_{rr} - \tau_{\theta\theta}), \quad (2.1)$$

$$\rho\left(v_t + uv_r + \frac{v}{r}v_\theta + wv_z + \frac{uv}{r}\right) = -\frac{p_\theta}{r} + \partial_r\tau_{r\theta} + \frac{1}{r}\partial_\theta\tau_{\theta\theta} + \partial_z\tau_{\theta z} + \frac{2}{r}\tau_{r\theta}, \quad (2.2)$$

and

$$\rho\left(w_t + uw_r + \frac{v}{r}w_\theta + ww_z\right) = -p_z - g + \partial_r\tau_{zr} + \frac{1}{r}\partial_\theta\tau_{\theta z} + \partial_z\tau_{zz} + \frac{\tau_{rz}}{r}, \quad (2.3)$$

$$\frac{1}{r}\partial_r(ru) + \frac{1}{r}v_\theta + w_z = 0 \quad (2.4)$$

and

$$\rho c_p\left(T_t + uT_r + \frac{v}{r}T_\theta + wT_z\right) = \tfrac{1}{2}\tau_{ij}\dot{\gamma}_{ij} + \mathscr{K}\left[\frac{1}{r}\partial_r(rT_r) + \frac{1}{r^2}T_{\theta\theta} + T_{zz}\right], \quad (2.5)$$

where τ_{ij} denote the deviatoric stresses, $\dot{\gamma}_{ij}$ is twice the rate-of-strain tensor ($\partial u_i/\partial x_j + \partial u_j/\partial x_i$ in Cartesian coordinates), g is gravity, c_p is specific heat and $\mathscr{K}$ is the conductivity. The subscripts (r, θ, z) denote partial derivatives, except in the case of the stress components, τ_{ij}, and then we use the notation ∂_r, and so on.

2.1. *Constitutive relations*

To model the non-Newtonian properties of the lava or analogue material, we use the Herschel–Bulkley constitutive relation. This choice is motivated as follows. The microstructural explanation for a yield stress is that, in static fluid, suspended particles or crystals become organized into an ordered structure held together by inter-particle forces. This structure is able to resist weak stress before it breaks apart and flows, hence providing the material yield strength. However, microstructure typically does not instantaneously disintegrate as the fluid flows. Rather, material structure is progressively broken up by increasing shear stresses. As a result of this more gradual attrition of microstructure, the fluid is *shear thinning* above the yield point, with a nonlinear relationship between the stresses and strain rates. The simplest fluid model that captures this kind of behaviour is the Herschel–Bulkley constitutive model. The model adequately describes many viscoplastic fluids, such as clay–water slurries and muds, and rheological measurements suggest that it reproduces properties of lava (Spera, Borgia & Strimple 1988; Pinkerton & Norton 1995).

The Herschel–Bulkley model is written as

$$\left.\begin{array}{ll} \tau_{ij} = (K\dot{\gamma}^n + \tau_p)\dot{\gamma}_{ij}/\dot{\gamma} & \text{for } \tau \geqslant \tau_p \\ \dot{\gamma}_{ij} = 0 & \text{for } \tau < \tau_p, \end{array}\right\} \quad (2.6)$$

where $\tau = \sqrt{\tau_{jk}\tau_{jk}/2}$, $\dot{\gamma} = \sqrt{\dot{\gamma}_{jk}\dot{\gamma}_{jk}/2}$, τ_p is the yield stress, the consistency K provides

a measure of resistance to shear, and n is the index. If $n < 1$ ($n > 1$), the fluid is shear thinning (thickening). The kaolin slurries used in laboratory experiments show a very marked nonlinear stress–strain-rate behaviour (see paper I): $n \approx \frac{1}{3}$. For magmas, viscometric studies suggest $\frac{1}{2} < n < 1$ (Spera *et al.* 1988; Pinkerton & Norton 1995).

The Herschel–Bulkley model was developed for isothermal viscoplastic materials, and must be generalized to account for temperature dependence. For many materials, the dominant effect of temperature is on the viscosity (consistency). However, for lava, the concentration of the crystals that provide the principal non-Newtonian effects gradually increases on lowering the temperature as the silicates crystallize in the magma. Not only does this have a significant effect on the viscosity, but it can also dramatically alter the yield stress. Thus, to generalize the rheological model we replace the constants K and τ_p by some prescribed functions of temperature: $K = K(T)$ and $\tau_p = \tau_p(T)$. We could, in addition, allow the index n to vary with temperature, but in the interest of simplicity (and absence of rheological data) we fix n. Moreover, because the temperature dependence of the density and conductivity is usually weaker than the (often exponential) dependence of the viscosity, we take $\mathscr{K}$ and ρ to be constant.

Although we do not need to specify the temperature dependence for the thin-layer theory, we adopt the illustrative model

$$K(T) = K_* \, \mathrm{e}^{-\tilde{G}(T-T_a)} \quad \text{and} \quad \tau_p(T) = \tau_{p*} \, \mathrm{e}^{-\tilde{S}(T-T_a)}, \tag{2.7}$$

where K_* and τ_{p*} are the values evaluated at the ambient temperature, T_a, and $\tilde{G}$ and $\tilde{S}$ are prescribed constants. Such exponential forms for the temperature dependence are commonly used for lavas (Shaw 1969; McBirney & Murase 1984; Spera *et al.* 1988; Pinkerton & Norton 1995), laboratory analogues (figure 5 of Fink & Griffiths 1990; Stasiuk *et al.* 1993), mud (Annis 1967; Briscoe, Luckham & Ren 1994), ice sheets (Hutter 1983), polymer processing (Tanner 1985) and suspensions (Aral & Kalyon 1984). These relations are often justified theoretically because the Arrhenius reaction rate has exponential form in the Frank–Kamenetskii approximation.

2.2. *Boundary conditions*

For the velocity field, we impose

$$u = v = 0, \quad w = w_s(r,t) \quad \text{on } z = 0, \tag{2.8}$$

where $w_s(r,t)$ is a prescribed axisymmetric source function. We also take the plate beneath the fluid to be thermally insulated: $T_z(r,\theta,z=0,t) = 0$. But, in the vent, fluid effuses upwards at the 'eruption temperature', T_e, which constitutes an incoming heat flux across $z = 0$. By balancing thermal diffusion above the vent with the heat flux across $z = 0$, we deduce that

$$\mathscr{K} T_z(r,\theta,z=0_+,t) = \rho c_p w_s [T(r,\theta,z,t)]_{z=0_-}^{z=0_+} = \rho c_p (T - T_e) w_s. \tag{2.9}$$

The surface of the dome, $z = h(r,\theta,t)$, is free:

$$h_t + [u h_r + v h_\theta / r]_{z=h} = w\,|_{z=h} \tag{2.10}$$

and

$$\begin{pmatrix} \tau_{rr} - p & \tau_{r\theta} & \tau_{rz} \\ \tau_{r\theta} & \tau_{\theta\theta} - p & \tau_{\theta z} \\ \tau_{zr} & \tau_{\theta z} & \tau_{zz} - p \end{pmatrix}_{z=h} \begin{pmatrix} -h_r \\ -h_\theta / r \\ 1 \end{pmatrix} = \begin{pmatrix} 0 \\ 0 \\ 0 \end{pmatrix}. \tag{2.11}$$

The surface thermal boundary conditions take the form,

$$F(T) = -\mathscr{K}\boldsymbol{n}\cdot\nabla T, \tag{2.12}$$

where $\boldsymbol{n}$ is the outward-pointing normal. Various forms are possible for the heat flux $F(T)$, depending on the specific physical conditions. For lava, if the dominant heat loss is thermal radiation, the Stefan–Boltzmann black-body law is appropriate, but forced convection of heat by wind can also be appreciable (Neri 1998). For experimental slurries, domes are cooled by conduction and convection in overlying water. The characterization of the cooling becomes especially involved when convection is turbulent. We avoid these complications here by selecting a simple model, Newton's law of cooling:

$$F(T) = a(T - T_a), \tag{2.13}$$

where a is a constant and T_a is the ambient temperature to which the fluid cools. If the temperature drop is small, this model is a first approximation to any cooling law. For completeness, and also to judge the importance of their effect later, we also quote the radiative and convective fluxes:

$$F_R(T) = \mathscr{E}\sigma(T^4 - T_a^4) \quad \text{and} \quad F_C(T) = \gamma\rho_a c_a \left(\frac{g\alpha_a\kappa_a^2}{\nu_a}\right)^{1/3}(T - T_a)^{4/3}, \tag{2.14}$$

where σ is the Stefan–Boltzmann constant and $\mathscr{E}$ is the emissivity (a positive constant less than unity), $\rho_a, c_a, \alpha_a, \kappa_a, \nu_a$ reflect the physical properties of the ambient fluid, and γ is an empirical constant, usually set to 0.1 (Griffiths & Fink 1997).

3. Non-dimensionalization

We remove dimensions from the equations as follows: we take a characteristic thickness of the fluid layer, H, as the dimension of z, and L to denote a horizontal length scale. We measure the speeds u and v by V, and w by HV/L, time by L/V, and pressure by ρgH. The temperature field is non-dimensionalized using the temperature drop between eruption and ambient temperature:

$$T = T_a + (T_e - T_a)\Theta \equiv T_a + \Delta T\Theta. \tag{3.1}$$

Next, let

$$\eta = \frac{K_* V^{n-1}}{H^{n-1}} \quad \text{and} \quad V = \frac{\rho g H^3}{\eta L}, \tag{3.2}$$

where K_* is the characteristic value of $K(T)$ at $T = T_a$. In dimensionless form, the governing equations then become

$$\epsilon^2 Re\left(u_t + uu_r + \frac{v}{r}u_\theta + wu_z - \frac{v^2}{r}\right) = -p_r + \epsilon\partial_r\tau_{rr} + \epsilon\frac{1}{r}\partial_\theta\tau_{r\theta} + \partial_z\tau_{rz} + \epsilon\frac{1}{r}(\tau_{rr} - \tau_{\theta\theta}), \tag{3.3}$$

$$\epsilon^2 Re\left(v_t + uv_r + \frac{v}{r}v_\theta + wv_z + \frac{uv}{r}\right) = -\frac{p_\theta}{r} + \epsilon\partial_r\tau_{r\theta} + \epsilon\frac{1}{r}\partial_\theta\tau_{\theta\theta} + \partial_z\tau_{\theta z} + \epsilon\frac{2}{r}\tau_{r\theta}, \tag{3.4}$$

$$\epsilon^4 Re\left(w_t + uw_r + \frac{v}{r}w_\theta + ww_z\right) = -p_z - 1 + \epsilon^2\partial_r\tau_{zr} + \epsilon^2\frac{1}{r}\partial_\theta\tau_{\theta z} + \epsilon\partial_z\tau_{zz} + \epsilon^2\frac{\tau_{rz}}{r}, \tag{3.5}$$

$$\frac{1}{r}\partial_r(ru) + \frac{1}{r}v_\theta + w_z = 0 \tag{3.6}$$

and

$$\Theta_t + u\Theta_r + \frac{1}{r}v\Theta_\theta + w\Theta_z = \tfrac{1}{2}\beta\tau_{ij}\dot\gamma_{ij} + \frac{\kappa}{\epsilon^2}\left[\Theta_{zz} + \epsilon^2\frac{1}{r}\partial_r(r\Theta_r) + \epsilon^2\frac{1}{r^2}\Theta_{\theta\theta}\right]. \tag{3.7}$$

A number of dimensionless parameters now appear. These are the aspect ratio of the fluid, ϵ, the Reynolds number, Re, an inverse Péclet number, κ, and the Brinkman number, β:

$$\epsilon = \frac{H}{L}, \quad Re = \frac{\rho V L}{\eta}, \quad \kappa = \frac{\mathscr{K}}{\rho c_p V L}, \quad \beta = \frac{\eta L V}{H^2 \rho c_p \Delta T}. \tag{3.8}$$

With the units V/H and $\rho g H^2/L$ for the strain rates and stresses, the constitutive relations become

$$\dot\gamma_{ij} = \begin{pmatrix} 2\epsilon u_r & \epsilon[(u_\theta - v)/r + v_r] & u_z + \epsilon^2 w_r \\ \epsilon[(u_\theta - v)/r + v_r] & 2\epsilon(u + v_\theta)/r & v_z + \epsilon^2 w_\theta/r \\ u_z + \epsilon^2 w_r & v_z + \epsilon^2 w_\theta/r & 2\epsilon w_z \end{pmatrix} \tag{3.9}$$

and

$$\tau_{ij} = \left[\mathscr{A}(\Theta)\dot\gamma^{n-1} + \frac{\mathscr{B}(\Theta)}{\dot\gamma}\right]\dot\gamma_{ij} \quad \text{if } \tau > \mathscr{B}(\Theta), \tag{3.10}$$

where

$$\mathscr{A}(\Theta) = \frac{K(T)}{K_*}, \quad \mathscr{B}(\Theta) = B\frac{\tau_p(T)}{\tau_{p*}} \tag{3.11}$$

and

$$B = \frac{\tau_{p*}H}{\eta V} \equiv \frac{\tau_{p*}L}{\rho g H^2}. \tag{3.12}$$

We refer to B as the Bingham number. For our illustrative model, $\mathscr{A} = \exp(-G\Theta)$ and $\mathscr{B} = B\exp(-S\Theta)$, where $G = \tilde G\Delta T$ and $S = \tilde S\Delta T$.

In non-dimensional variables the boundary conditions become

$$u = 0, \quad v = 0, \quad w = w_s(r,t), \quad \kappa\Theta_z = \epsilon^2(\Theta - 1)w_s(r,t) \quad \text{on } z = 0, \tag{3.13}$$

and

$$\left.\begin{aligned} h_t + uh_r + vh_\theta/r &= w \\ \tau_{rz} + ph_r &= \epsilon h_r\tau_{rr} - \epsilon\tau_{r\theta}h_\theta/r \\ \tau_{\theta z} + ph_\theta/r &= \epsilon h_r\tau_{r\theta} + \epsilon\tau_{\theta\theta}h_\theta/r \\ p &= \epsilon(\tau_{zz} - \epsilon h_r\tau_{rz}) - \epsilon h_\theta\tau_{\theta z}/r \\ \kappa(\Theta_z - \epsilon^2 h_r\Theta_r - \epsilon^2 h_\theta\Theta_\theta/r^2) &= -\epsilon^2\alpha\Theta\sqrt{1 + \epsilon^2 h_r^2 + \epsilon^2 h_\theta^2/r^2} \end{aligned}\right\} \quad \text{on } z = h(r,\theta,t), \tag{3.14}$$

where α is a parameter measuring the degree of surface cooling:

$$\alpha = \frac{aL}{\rho c_p V H}. \tag{3.15}$$

More detailed models of the surface thermal boundary condition can be incorporated in (3.14) by taking α to depend on Θ. For example, the convective and radiative flux

Constants	Silicic lava	Basaltic lava	Wax	Wax–kaolin slurry	Syrup
Density, ρ (kg m^{-3})	2600	2600	1126	1450	1438
Viscosity, η (Pa s)	10^9	10^4	0.18	0.78	10^5
Yield stress, τ_p (Pa)	10^5	10^2	0	84	0
Specific heat, c_p (J kg^{-1} °C^{-1})	1150	1200	2500	1800	2059
Conductivity, $\mathscr{K}$ (J m^{-1} s^{-1} °C^{-1})	1.26	2	0.218	0.365	0.358

TABLE 1. Physical constants. The data for lava are taken from Griffiths & Fink (1993), McBirney & Murase (1984), Pinkerton & Norton (1995) and Shaw (1969). The data for wax and the wax–kaolin slurry are taken from Griffiths & Fink (1997) and those for syrup from Stasiuk *et al.* (1993). The characteristic value of viscosity corresponds to the maximal value at the low end of the temperature range.

Extrusion conditions	Silicic lava	Basaltic lava	Wax and slurry	Syrup
Dome radius, L (m)	10^2	10^3	0.10	0.5
Effusion rate, Q (m^3 s^{-1})	1	10	10^{-6}	10^{-6}
Eruption temperature, T_e (°C)	1100	1400	21	21
Typical temperature drop, ΔT (°C)	300	300	10	30

TABLE 2. Typical extrusion conditions. The data for lava are taken from Griffiths & Fink (1993), McBirney & Murase (1984) and Shaw (1969); the temperature drop assumes that cooling lowers the temperature to the solidification value, below which our approximations break down. The data for wax and the wax–kaolin slurry are taken from Griffiths & Fink (1997), and for corn syrup from Stasiuk *et al.* (1993).

laws in (2.14) can be written as

$$\alpha(\Theta) = \begin{cases} \alpha_R[(1 + \Theta\Delta T/T_a)^4 - 1] \\ \alpha_C \Theta^{4/3} \end{cases} \tag{3.16}$$

respectively, where

$$\alpha_R = \frac{\mathscr{E}\sigma L T_a^4}{\rho c_p H V \Delta T} \quad \text{and} \quad \alpha_C = \frac{\gamma \rho_a c_a L}{\rho c_p V H}\left(\frac{g\alpha_a \kappa_a^2 \Delta T}{\nu_a}\right)^{1/3}. \tag{3.17}$$

Though it is straightforward to deal with these more complicated thermal boundary conditions, we do not use them in our numerical computations because they do not qualitatively change the predictions of the theory.

3.1. *Non-dimensional parameters*

In tables 1 and 2 we summarize the physical constants and extrusion conditions typical for lava and experiments. From these data we can derive rough, order-of-magnitude estimates of the non-dimensional parameters; see table 3, for $n = 1$. These estimates are obtained by connecting the dimensional (Q) and dimensionless (q) extrusion rates,

$$Q = LHVq, \tag{3.18}$$

together with the relation,

$$H = \left(\frac{K_* L^{1-n} Q^n}{\rho g q^n}\right)^{1/(2n+2)} \quad \left(= \left[\frac{\eta_* Q}{\rho g q}\right]^{1/4} \quad \text{if } n = 1 \right), \tag{3.19}$$

that follows from eliminating V from (3.18) using equation (3.2).

Parameter		Silicic lava	Basaltic lava	Wax and slurry	Syrup
ϵ	$(\eta Q/\rho g q L^4)^{1/4}$	0.1	0.001	0.01	0.1
Re	$(\rho^5 g Q^3/\eta^5 q^3)^{1/4}$	10^{-7}	1	1	10^{-7}
B	$\tau_{p*} L(q/\eta\rho g Q)^{1/2}$	3	0	0 and 100	0
κ	$(\eta q^3/\rho g Q^3)^{1/4}\mathscr{K}/\rho c_p$	10^{-5}	10^{-7}	0.001	0.01
β	$(\rho^3 g^3 \eta Q/q)^{1/4}/\rho c_p \Delta T$	10^{-4}	10^{-5}	10^{-6}	10^{-5}
G	$\tilde{G}\Delta T$	10–18	5	1	7

TABLE 3. Typical values of non-dimensional numbers, given the physical constants and extrusion conditions in tables 1 and 2, assuming $n = 1$ and $q = \pi$. The values of $\tilde{G}$ are estimated from data given by McBirney & Murase (1984), Fink & Griffiths (1990) and Stasiuk *et al.* (1993). The parameter G is assumed to be equal for both wax and the wax–kaolin slurry. If we take T_α to measure the atmospheric temperature, rather than the lava solidification temperature, then β is 3.5 times smaller and G is 3.5 times larger for silicic and basaltic lava.

Lastly, there is a further dimensionless parameter in the boundary conditions that measures the cooling rate. Our Newton cooling law is a simple prescription that has meaning only as an approximation to a radiative or convective cooling law. Hence, to gauge the importance of cooling, we estimate α_R and α_C: based on the numbers given in tables 1 and 2, and supplemented by data given by Griffiths & Fink (1997), we find that α_R and α_C are order unity for $q = \pi$.

A key observation is that ϵ, the aspect ratio, is small for the domes we study; in the next section, we exploit this small parameter to derive a reduced description of the problem. We also take Re to be order unity or less, guided by the slow evolution of the lava and experimental domes, and the Brinkman number, characterizing frictional heating, to be negligible (see table 3).

The only thorn in our side is the low value of the conductivities suggested by the estimates in table 3. Strictly speaking, the asymptotic expansion takes the limit $\epsilon \to 0$ with κ order one, and is not compatible with the data in the table which suggest that $\kappa < \epsilon$ for all the materials of interest. However, as mentioned later, the main parameter that must be large in order to follow the asymptotic pathway is the ratio κ/ϵ^2 (the factor in front of the vertical diffusion term in the heat equation). Unfortunately, even with this rescaling of κ, the theory is still inapplicable to lava (and corn syrup); we delve into the physical meaning of this later.

For wax and clay–wax slurries, on the other hand, the rescaling appears to justify the asymptotic analysis. However, although our theory predicts that $\epsilon \sim 10^{-2}$ for Griffiths & Fink's experiments, direct measurements of H/L suggest values of 0.1 or larger. Such values for ϵ would push us into a regime where κ/ϵ^2 is actually small, and the theory is therefore inapplicable. In this regard, it is important to appreciate that in the theory, H and L are not independent parameters, but are connected through the effusion rate, Q. It is this connection that provides the estimate of ϵ. We have two possible explanations for the discrepancy. First, there are factors of order unity floating around, and it only takes a factor of five or so to bring our theoretical estimate up to a value of 0.1; in principle, such factors are contained in the theory, and do not necessarily imply that the analysis breaks down. Second, the maximal heights are reached over the vent, which is where the asymptotic analysis formally breaks down; perhaps the discrepancy reflects a failure of lubrication theory.

Thus, although a direct estimate of κ/ϵ^2 from the tables appears to justify our theory with regard to experiments, we should be more cautious. The theory is probably marginal at best; perhaps it works well for a subset of the experiments, but it may only crudely model the remainder. Nonetheless, because no other theory is available, we press on with the current analysis in order to provide at least one theoretical benchmark.

4. Thin-layer theory

In this section we exploit the small aspect ratio of the dome ($\epsilon \ll 1$) to reduce the governing equations. We begin by substituting the asymptotic sequences,

$$u = u_0 + \epsilon u_1 + \cdots, \quad v = v_0 + \epsilon v_1 + \cdots, \quad w = w_0 + \epsilon w_1 + \cdots, \quad \Theta = \Theta_0 + \epsilon \Theta_1 + \cdots, \tag{4.1}$$

into the governing equations and then gather together terms of the same order in ϵ. This generates a hierarchy of equations that we solve order by order, beginning with order ϵ^0:

$$p_{0r} = \partial_z \tau_{0rz}, \quad \frac{1}{r} p_{0\theta} = \partial_z \tau_{0\theta z}, \quad p_{0z} = -1, \tag{4.2}$$

$$\frac{1}{r}\partial_r (r u_0) + \frac{1}{r} v_{0\theta} + w_{0z} = 0, \quad \Theta_{0zz} = 0 \tag{4.3}$$

and

$$\begin{pmatrix} \tau_{0rz} \\ \tau_{0\theta z} \end{pmatrix} = \frac{1}{\dot\gamma_0} \left[\mathscr{A}(\Theta_0) \dot\gamma_0^n + \mathscr{B}(\Theta_0) \right] \begin{pmatrix} u_{0z} \\ v_{0z} \end{pmatrix} \quad \text{for } \mathscr{B}(\Theta_0) < \tau_0, \tag{4.4}$$

$$u_{0z} = v_{0z} = 0 \quad \text{for } \mathscr{B}(\Theta_0) > \tau_0, \tag{4.5}$$

where

$$\tau_0 \equiv \sqrt{\tau_{0rz}^2 + \tau_{0\theta z}^2} \quad \text{and} \quad \dot\gamma_0 = \sqrt{u_{0z}^2 + v_{0z}^2}. \tag{4.6}$$

We similarly deal with the boundary conditions, which provide the leading-order relations,

$$u_0 = v_0 = 0, \quad w_0 = w_s(r,t), \quad \Theta_{0z} = 0 \quad \text{on } z = 0 \tag{4.7}$$

and

$$h_{0t} + u_0 h_{0r} + v_0 h_{0\theta}/r = w_s(r,t), \quad \tau_{0rz} = \tau_{0\theta z} = p_0 = \Theta_{0z} = 0 \quad \text{on } z = h_0(r,\theta,t). \tag{4.8}$$

The leading-order heat equation has the solution, $\Theta_0 = \Theta_0(r,\theta,t)$, indicating that the dome is isothermal in the vertical. This is a vital simplification; we return to consider cases in which we cannot make this approximation in § 7. The remainder of the leading-order equations fix the vertical structure:

$$p_0 = h_0 - z, \quad \tau_{0rz} = -h_{0r}(h_0 - z), \quad \tau_{0\theta z} = -h_{0\theta}(h_0 - z)/r. \tag{4.9}$$

Because $\tau_0 = (h_0 - z)\sqrt{h_{0r}^2 + h_{0\theta}^2/r^2}$ decreases with z, the largest shear stress occurs along the base of the fluid; this must exceed $\mathscr{B}(\Theta_0)$ in order for the fluid to move. But, $\tau_0 = 0$ at $z = h_0$, and so the stress falls beneath the yield stress at a level $z = Y_0(r,\theta,t)$. We refer to this level as the yield surface, and the fluid is locally in motion if $Y_0 > 0$.

Below the yield surface, $z < Y_0$, we have

$$\begin{pmatrix} u_{0z} \\ v_{0z} \end{pmatrix} = -(h_{0r}^2 + h_{0\theta}^2/r^2)^{(1-n)/2n} \mathscr{A}^{-1/n} (Y_0 - z)^{1/n} \begin{pmatrix} h_{0r} \\ h_{0\theta}/r \end{pmatrix}. \tag{4.10}$$

Above this surface, $z > Y_0$, the fluid is rigid to leading order and $u_{0z} = v_{0z} = 0$. However, this is not a true 'plug flow'–a more refined asymptotic analysis reveals that this region is weakly yielding (Balmforth & Craster 1999), and sufficiently so to account for the radial expansion of the dome. A better terminology is to refer to this region as a 'pseudo-plug'.

We next formulate the vertical integrals of $u_0(r,\theta,z,t)$ and $v_0(r,\theta,z,t)$:

$$\mathscr{U}(r,\theta,t) = \int_0^{h_0} u_0(r,\theta,z,t)\,dz \quad \text{and} \quad \mathscr{V}(r,\theta,t) = \int_0^{h_0} v_0(r,\theta,z,t)\,dz. \tag{4.11}$$

By using the leading-order solution, we may explicity evaluate these integrals. An evolution equation for $h_0(r,\theta,t)$ is then derived by integrating the continuity equation and using $\mathscr{U}$, $\mathscr{V}$ and the free-surface boundary condition. The result, given below as equation (4.14), is one of the key equations in our thin-layer theory. A second equation is formulated by proceeding to higher order in the expansion, and specifically taking $\Theta_1 = 0$ and considering the order-ϵ^2 terms of the heat equation:

$$\kappa\Theta_{2zz} = \Theta_{0t} + u_0\Theta_{0r} + \frac{v_0}{r}\Theta_{0\theta} - \frac{1}{r}\kappa\partial_r(r\Theta_{0r}) - \frac{1}{r^2}\kappa\Theta_{0\theta\theta} + \beta\left(u_0h_{0r} + \frac{1}{r}v_0h_{0\theta}\right). \tag{4.12}$$

The integral of this equation from $z = 0$ to h_0, together with the boundary conditions,

$$\left.\begin{aligned} &\kappa\Theta_{2z} = w_s(\Theta_0 - 1) && \text{on } z = 0 \\ &\kappa(\Theta_{2z} - h_{0r}\Theta_{0r} - h_{0\theta}\Theta_{0\theta}/r^2) = \alpha\Theta_0 && \text{on } z = h_0(r,\theta,t), \end{aligned}\right\} \tag{4.13}$$

provides an equation for Θ_0, which appears below as (4.15).

4.1. *The thin-layer model*

We summarize the results of the expansion by quoting the thin-layer equations in all their glory:

$$h_t + \frac{1}{r}\partial_r(r\mathscr{U}) + \frac{1}{r}\mathscr{V}_\theta = w_s, \tag{4.14}$$

and

$$\Theta_t + \frac{\mathscr{U}}{h}\Theta_r + \frac{\mathscr{V}}{rh}\Theta_\theta = \frac{\kappa}{rh}\partial_r(rh\Theta_r) + \frac{\kappa}{r^2h}\partial_\theta(h\Theta_\theta) - \frac{\alpha}{h}\Theta + \frac{w_s}{h}(1-\Theta) - \frac{\beta}{h}\left(h_r\mathscr{U} + \frac{h_\theta}{r}\mathscr{V}\right), \tag{4.15}$$

where

$$\begin{bmatrix}\mathscr{U}(r,\theta,t)\\ \mathscr{V}(r,\theta,t)\end{bmatrix} = -\frac{n(h_r^2 + h_\theta^2/r^2)^{(1-n)/2n}Y^{1+1/n}}{(n+1)\mathscr{A}(\Theta)^{1/n}}\left(h - \frac{nY}{2n+1}\right)\begin{bmatrix}h_r\\ h_\theta/r\end{bmatrix} \tag{4.16}$$

and

$$Y = \left[h - \frac{\mathscr{B}(\Theta)}{\sqrt{h_r^2 + h_\theta^2/r^2}}\right]_+. \tag{4.17}$$

Here we have dropped the zero subscript on the understanding that each variable hereafter refers to the leading-order term, and incorporated the yield condition into the definition of Y (the subscript $+$ in (4.17) implies we take the value of the quantity only where it is positive and zero elsewhere). From hereon we ignore the viscous heating term in equations (4.15) because the parameter β is small (see table 3) for

all the materials we have in mind. However, for some polymeric materials relevant for thermosetting plastics, the effects of viscous heating can be large (Pearson 1977). The inverse Péclet number κ is also small and is a candidate for omission on similar grounds. But this parameter multiplies the highest derivative terms in (4.15) and hence we retain it because of its regularizing effect.

5. Cooling axisymmetrical domes

We now present some results of the thin-layer model for cooling axisymmetrical domes. In this case, we set $\partial_\theta \to 0$, drop the θ argument and take $\mathscr{V} = 0$. The equations are then solved using the numerical scheme described in paper I, with initial conditions, $h(r,0) = 10^{-3}\exp(-r^2/25)$ and $\Theta(r,0) = 0$, and radial boundary conditions, $h_r(0,t) = h_r(r_\infty,t) = \Theta_r(0,t) = \Theta(r_\infty,t) = 0$ (r_∞ is a radius that is sufficiently far from the vent to ensure that the outer boundary condition has no effect). For the source, we prescribe the incoming flux and vent radius: $w_s(r,t) = 0.1(r_*^2 - r^2)\vartheta(r_*^2 - r^2)$ and $r_* = 0.15$. Note that $q \sim 10^{-4}$ (rather than order one, as assumed in table 3), so the extrusion time is relatively long. We choose this small extrusion rate because the dome height and radius are then order-one numbers but the vent radius is small. If we take q order unity, the vent radius is order one and the dome proportions can become numerically large.

We also focus on thermal effects rather than variations in B and n. The effect of these parameters is similar to the isothermal problem (paper I). In that case, the yield stress dominates once $B \sim 0.1$, and one encounters Newtonian-like behaviour for $B \sim O(10^{-5})$ (with $w_s(r,t)$ chosen as above). Also, the shear thinning of the fluid can have similar effects to a yield stress.

5.1. *Representative solutions*

To illustrate the typical features of evolving non-isothermal domes, we describe three representative cases with $\mathscr{B}(\Theta) = B$ and $\mathscr{A}(\Theta) = \exp(-G\Theta)$ (i.e. $S = 0$). This models a Herschel–Bulkley material with constant yield stress and temperature-dependent consistency, and is perhaps relevant to wax–kaolin slurries. The examples are computed for three values of α, with $B = 10^{-3}$, $G = 8$, $\kappa \ll 1$ and $n = 1$, and are shown in figures 1–3.

In all three cases, the temperature field evolves to a quasi-steady profile (in the final case the progress to this profile is very slow). Such a profile is possible because horizontal diffusion is relatively small in these models and $\mathscr{U}(r,t)$ becomes approximately steady (see figure 1*c*). At this stage of the dome expansion, there is then a local balance between surface cooling, advection and heat input:

$$\mathscr{U}\Theta_r \approx w_s(1-\Theta) - \alpha\Theta. \tag{5.1}$$

Thence, away from the vent,

$$\Theta \to \exp\left[-\alpha\int^r \mathrm{d}s/\mathscr{U}(s)\right], \tag{5.2}$$

which suggests that the thermal profile decays spatially at a rate proportional to α (but this ignores how thermal effects change $\mathscr{U}(r)$).

When the dome cools rapidly, advection is unimportant and

$$\Theta(r,t) \sim w_s(r,t)/[\alpha + w_s(r,t)]. \tag{5.3}$$

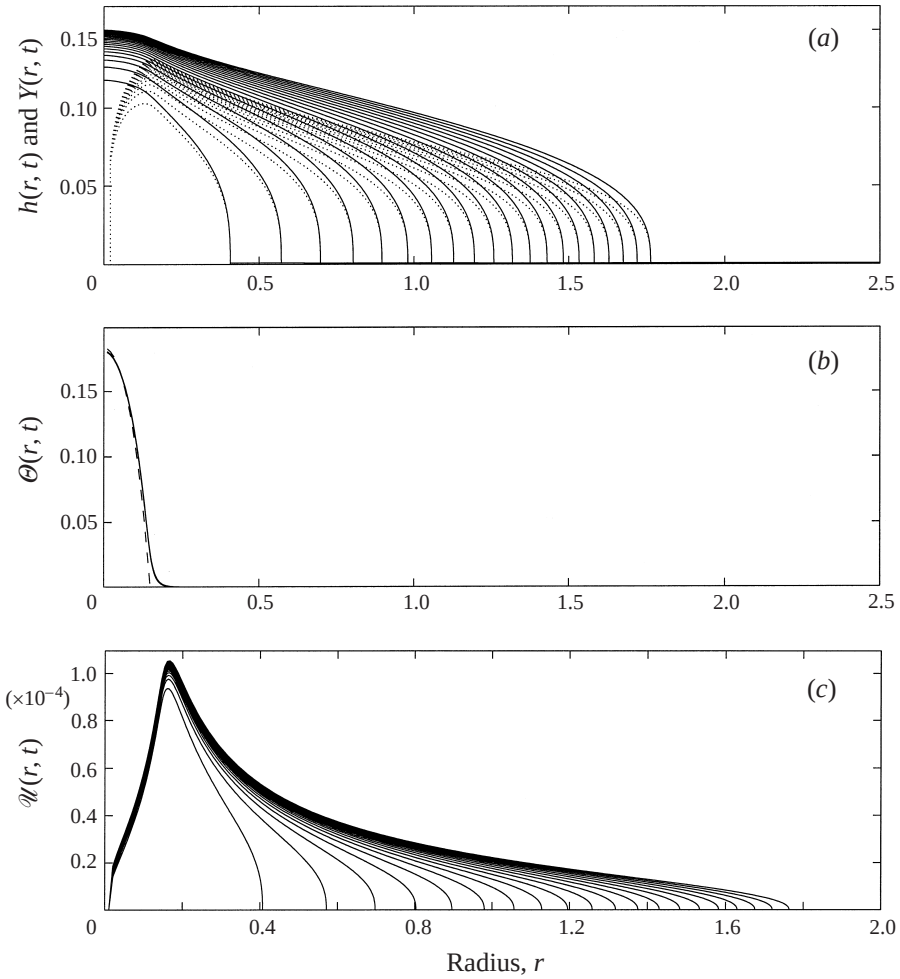

FIGURE 1. Dome and temperature evolution for $B = 10^{-3}$, $G = 8$, $\alpha = 0.01$, $\kappa = 10^{-5}$ and $n = 1$. (*a*) The height field at successive instants, spaced by 500 time units; the dotted curves show the corresponding yield surfaces, $Y(r,t)$. (*b*) The temperature field at the same instants. Also shown by the dashed line is the rapid cooling approximation given by (5.3). (*c*) $\mathscr{U}(r,t)$.

Temperature gradients are then concentrated at the vent (figure 1), and the temperature elsewhere falls to the ambient level. At the opposite extreme, there is little cooling and fluid expands outwards at the eruption temperature (see figure 3).

In both limits, the dome evolves isothermally. The cool dome in figure 1 is much like an isothermal dome with the same Bingham number. However, the hot dome is more like an isothermal dome with a Bingham number of 0.1. This is because the cool dome evolves at the background temperature and with the characteristic viscosity values used to compute B. At these viscosities, the fluid is almost Newtonian. However, the hot dome has an elevated temperature and an effective viscosity that is lower by a factor of about 10^4. This is equivalent to an increase in B of 100, as implied by the definition of the Bingham number in table 3 ($B \sim \eta^{-1/2}$). Thus the hot dome has an effective Bingham number of $100B = 0.1$, and is yield-stress-dominated.

The dome with an intermediate cooling rate is midway between the two extremes. As a result, the structure displays features characteristic of both the cool, almost

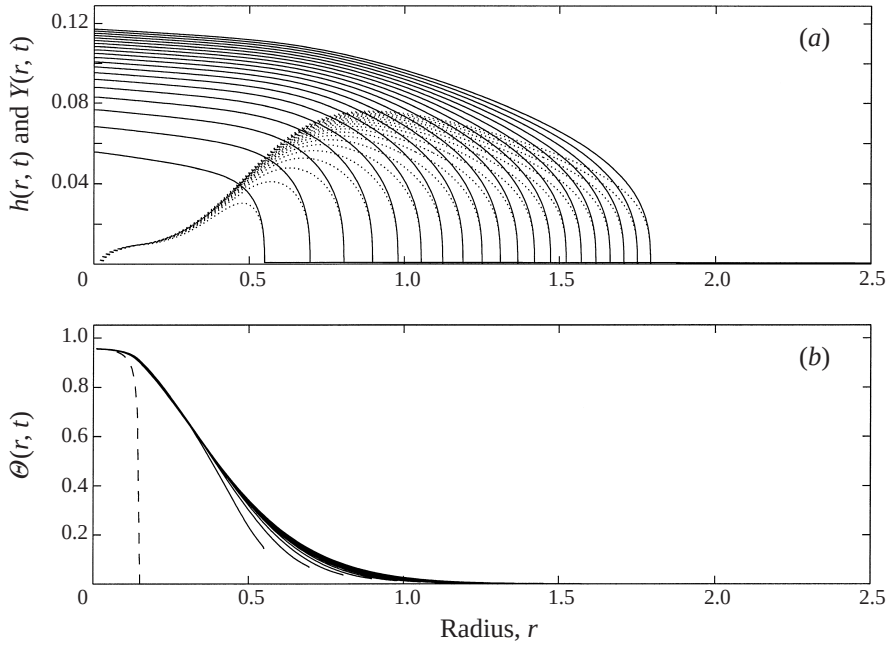

FIGURE 2. Dome and temperature evolution for $B = 10^{-3}$, $G = 8$, $\alpha = 10^{-4}$, $\kappa = 10^{-8}$ and $n = 1$. (*a*) and (*b*) As in figure 1.

Newtonian dome, and the hot, yield-stress-dominated dome. In particular, the quasi-steady temperature profile acts like a 'cooling front'. For radii inside this front, the dome is hot and yield-stress dominated. But beyond these radii, the fluid is almost Newtonian and cool. Note that we have engineered this behaviour by knowing the magnitude of the overall decrease in viscosity (essentially, G), and then judiciously selecting the Bingham number. Had we chosen a much smaller Bingham number, the fluid would have been approximately Newtonian, or if B had been larger, we would have seen yield-stress-dominated evolution.

5.2. *Radius and height scalings*

When the fluid is isothermal and extruded from a point source, there are simple scaling laws that characterize the radius and height of the dome in two particular limits of the fluid rheology (Huppert *et al.* 1982; Blake 1990): $R(t) \sim t^{1/2}$ and $h(0,t) \sim t^0$ for viscous fluid, and $R(t) \sim t^{2/5}$ and $h(0,t) \sim t^{1/5}$ for a fluid dominated by yield stress. In figure 4 we compare these scalings with the radius and height evolution of our representative domes.

As expected from the discussion above, the cool dome has Newtonian scalings (as mentioned in paper I, the height of a Newtonian dome does not perfectly follow the scaling $h(0,t) \sim t^0$ because the vent has finite size), and the hot dome has scalings close to those of the yield-stress-dominated case. The dome with an intermediate cooling rate initially follows a radius scaling much like the hot dome. But then, between times of 10^2 and 10^3, switches over to a scaling more like the cool dome. This switch occurs as the dome radius moves through the cooling front that forms at radii from 0.2 to 0.8. Therefore, in this particular case, the evolution of the radius and height displays cooling-induced transitions.

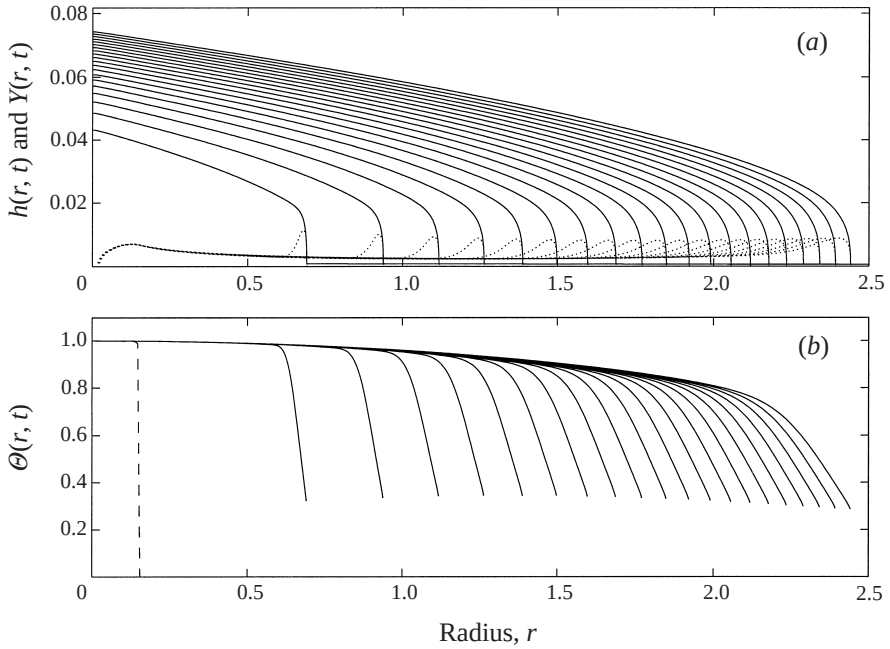

FIGURE 3. Dome and temperature evolution for $B = 10^{-3}$, $G = 8$, $\alpha = 10^{-6}$, $\kappa = 10^{-6}$ and $n = 1$. (*a*) and (*b*) As in figure 1.

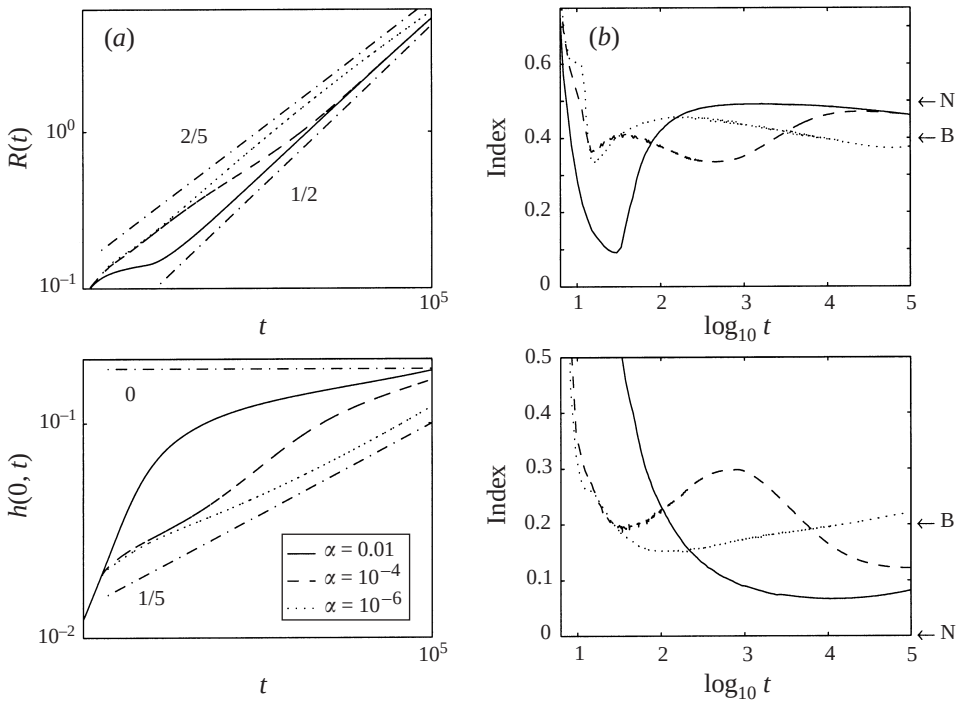

FIGURE 4. The variation of radius and height with time for the domes in figures 1–3. In (*b*) and (*d*) we show the indices of local 'power laws'. In (*a*) and (*c*) dot-dashed lines show the isothermal Newtonian and yield-stress-dominated scalings; these are labelled *N* and *B* in panels (*b*) and (*d*).

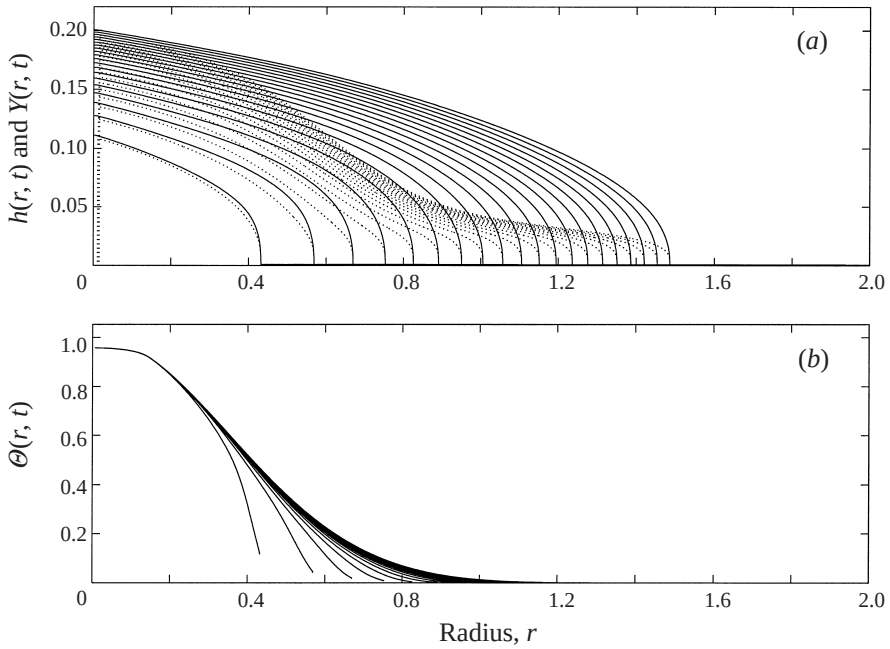

FIGURE 5. Dome and temperature evolution for $B = 0.01$, $G = S = 4$, $\alpha = 10^{-4}$, $\kappa = 10^{-6}$ and $n = 1$. (*a*) The height field at successive instants spaced by 500 time units; the dotted curves show the corresponding yield surfaces, $Y(r, t)$. (*b*) The temperature field at the same instants.

5.3. *Crystallization: temperature-dependent yield stresses*

The illustrative models above have a constant yield stress. There is some argument for this in the case of kaolin suspensions (particle concentration does not increase on lowering the temperature), though this may underestimate the effect of temperature on slurry microstructure (Annis 1967; Briscoe *et al.* 1994). But for silicic lavas, the lowering of the temperature induces a gradual crystallization of the silicates, and this must affect the yield stress. A crude way to incorporate crystallization is to use the Einstein–Roscoe relations (Pinkerton & Stevenson 1992) to define the material properties in terms of the concentration of crystals, and assume the particle concentration to follow an Arrhenius-type dependence on temperature. On using a Frank–Kamenetskii-style approximation, one then obtains the exponential forms, $\mathscr{A}(\Theta) = \exp(-G\Theta)$ and $\mathscr{B}(\Theta) = B\exp(-S\Theta)$, of our illustrative model.

A sample computation using $G = S = 4$ is shown in figure 5. The most striking feature of this picture is that the yield surfaces are highest inside the cooling front. This is exactly the reverse of what we see in figure 2 and reflects the fact that cooling has a more significant effect on the yield stress than the viscosity for these parameter values: though $\mathscr{A}$ and $\mathscr{B}$ have the same temperature dependence, the flow depends differently on $\mathscr{A}$ and $\mathscr{B}$. Indeed, the effective yield stress is $\mathscr{B}/\mathscr{A}^{1/2} \propto \exp(-2\Theta)$. Thus, the fluid has a strong yield stress outside the cooling front but is almost Newtonian inside.

Again, $R(t)$ and $h(0, t)$ display transitions that one can correlate with the passage of the dome radius through the cooling front. But this time we pass from Newtonian scalings to yield-stress-dominated ones.

6. Dome instability

When the viscosity depends strongly on temperature, axisymmetric domes can be prone to non-axisymmetric instabilities. The basic mechanism underlying this instability is tied to both the cooling law, $-\alpha\Theta/h$, and the temperature dependence of the viscosity. Essentially, a perturbation that locally decreases the height of the dome induces the fluid to cool more rapidly; thus the viscosity becomes higher and flow is locally reduced. Conversely, if the perturbation increases the dome thickness elsewhere, the cooling is less pronounced in those regions and the fluid surges forward. Thus, perturbations grow and create non-axisymmetrical structure as the cool regions slow down and the hot regions accelerate and draw more fluid into lobes behind them.

To explore this further, we consider an expanding, cooling, axisymmetric dome, denoted $\hat{h}(r,t)$, $\hat{\mathscr{U}}(r,t)$ and $\hat{\Theta}(r,t)$, and add infinitesimal perturbations, distinguished by a prime decoration and with angular dependence $\exp(\mathrm{i}m\theta)$:

$$h(r,\theta,t) = \hat{h}(r,t) + h'(r,t)\mathrm{e}^{\mathrm{i}m\theta}, \quad \Theta(r,\theta,t) = \hat{\Theta}(r,t) + \Theta'(r,t)\mathrm{e}^{\mathrm{i}m\theta}, \tag{6.1}$$

$$\mathscr{U}(r,\theta,t) = \hat{\mathscr{U}}(r,t) + \mathscr{U}'(r,t)\mathrm{e}^{\mathrm{i}m\theta} \quad \text{and} \quad \mathscr{V}(r,\theta,t) = \mathscr{V}'(r,t)\mathrm{e}^{\mathrm{i}m\theta}; \tag{6.2}$$

the integer wavenumber m must be varied to determine the stability of each azimuthal mode. After substituting these relations into the thin-layer equations, we find

$$h'_t + \frac{1}{r}\partial_r(r\mathscr{U}') + \frac{\mathrm{i}m}{r}\mathscr{V}' = 0 \tag{6.3}$$

and

$$\hat{h}\Theta'_t + h'\hat{\Theta}_t + \mathscr{U}'\hat{\Theta}_r + \hat{\mathscr{U}}\Theta'_r = \kappa\left[\frac{1}{r}\partial_r(rh'\hat{\Theta}_r + r\hat{h}\Theta'_r) - \frac{m^2}{r^2}\hat{h}\Theta'\right] - (\alpha + w_s)\Theta'. \tag{6.4}$$

These equations cannot be solved by the usual methods of linear stability theory (decomposition into normal modes) because the equilibrium state is inhomogeneous and time-dependent. Instead, we solve (6.3)–(6.4) as an initial-value problem for each m, using the same numerical scheme as before and the initial conditions

$$h'(r,0) = 0 \quad \text{and} \quad \Theta'(r,0) = 10^{-3}\exp(-r^2/5). \tag{6.5}$$

To determine whether non-axisymmetric instabilities are possible we specialize to a material with no yield stress and $n = 1$. Our results for axisymmetrical domes suggest that this case is likely to be most influenced by thermal effects and therefore unstable. The results are shown in figures 6–9, for $\kappa = 10^{-5}$ and $\alpha = 10^{-4}$.

Figure 6 displays the evolution of the equilibrium and perturbation for the $m = 3$ mode with $G = 8$. In this case a cooling front forms in the equilibrium dome, and, in the vicinity of the resulting temperature gradient, the perturbation amplifies in time. In other words, the dome is unstable; height perturbations at the cooling front feed a growing thermal perturbation.

The height perturbation, $h'(r,t)$, also develops a sharp peak at the periphery of the dome. This is a kinematic effect arising due to our Eulerian description of the perturbation; the sharp peak reflects the motion of the dome's edge. In fact, locally, the periphery of the dome is much like a travelling planar front with a neutral, translational eigenmode proportional to $\hat{h}_r$. That function is sharply peaked

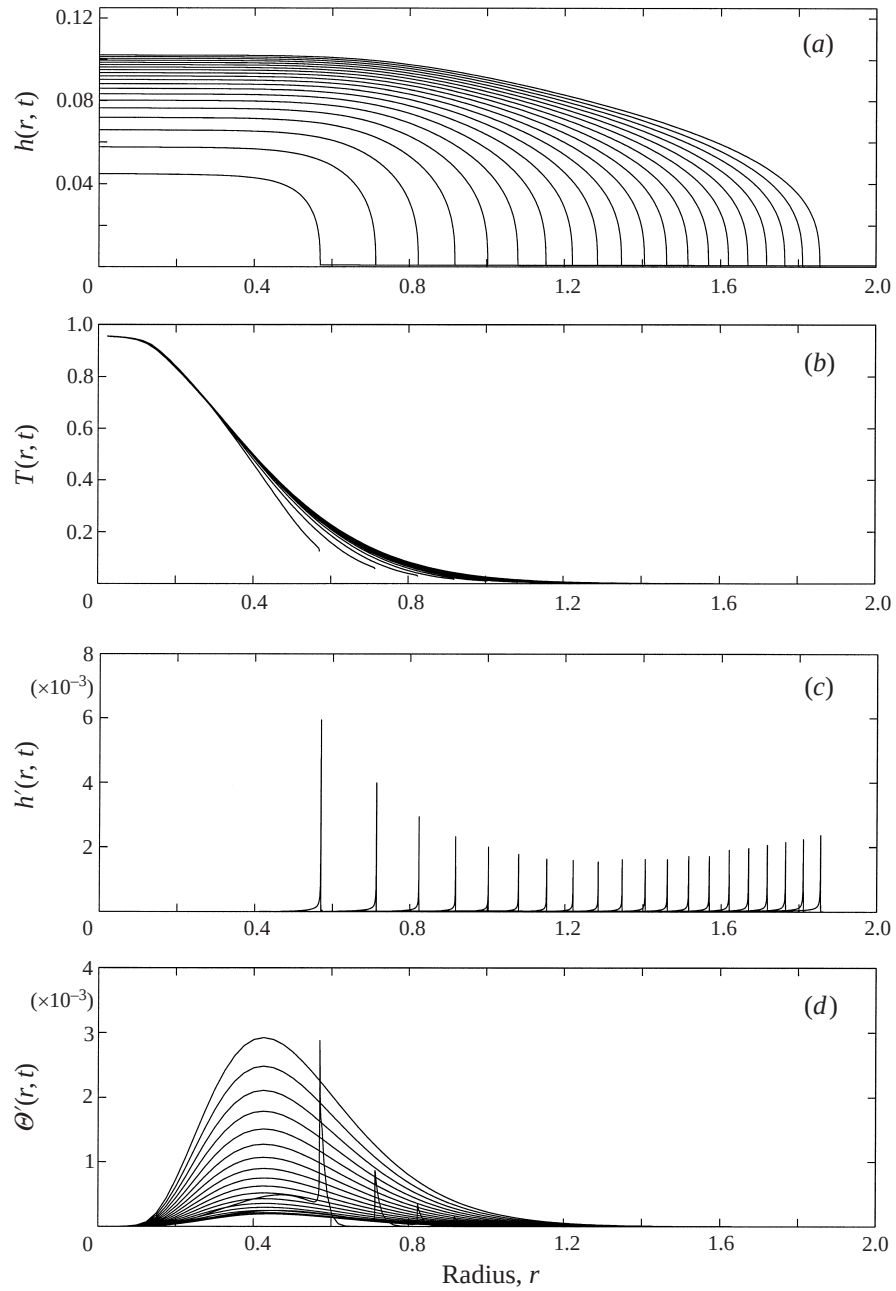

FIGURE 6. The evolution of the dome and temperature field for $m = 3$ with $\alpha = 10^{-4}$, $\kappa = 10^{-5}$ and $G = 8$; the curves show the solutions at successive instants spaced by 500 time units.

at our dome edge, but not singular due to our choice of initial condition ($\hat{h}$ remains finite 'outside' the dome). The form, $r\xi(t)e^{im\theta}\hat{h}_r(r,t)$, reproduces the structure of the perturbation near $r = R$.

At the end of the simulation we add the perturbation onto the equilibrium profile in figure 7 to gain an impression of the overall effect of the instability. Because this

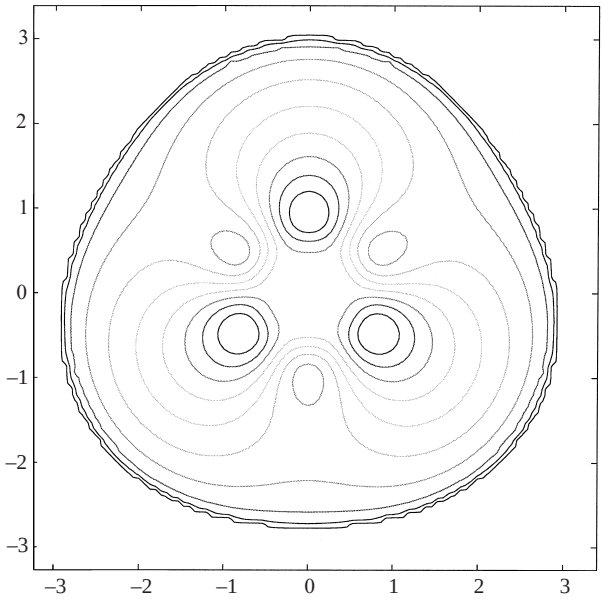

FIGURE 7. A contour plot of the height field produced when adding $50h'(r,t)$ to the axisymmetric solution. The parameters are $G = 8$, $m = 3$, $\alpha = 10^{-4}$ and $\kappa = 10^{-5}$ at time 2.5×10^4. The contours are at intervals of 0.15.

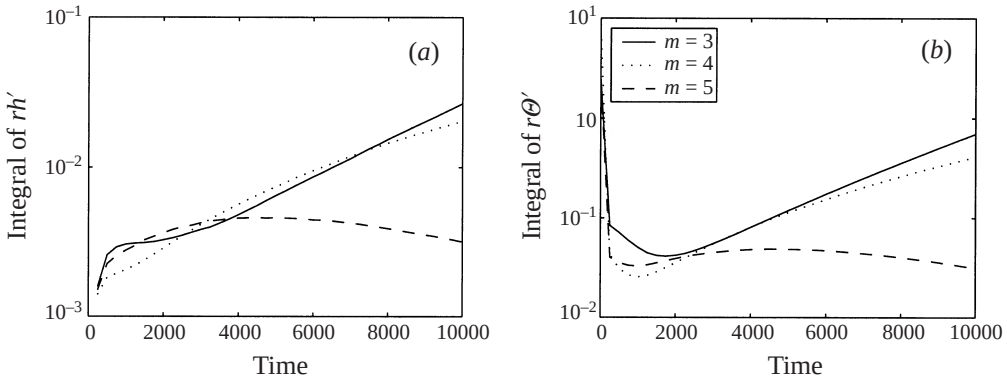

FIGURE 8. Integral measures of the perturbations for $G = 8$ and $m = 3, 4, 5$.

is a linear calculation, we have no way to compute the amplitude of the linear mode; instead we add in an arbitrary multiple, A, of the perturbation, guided mainly by aesthetics. We also subtract out the almost divergent part of $h'(r, te^{im\theta})$ by fitting the function $r\xi(t)e^{im\theta}\hat{h}_r(r,t)$ to the sharp peak near $r = R$ and then shifting the radial coordinate: $\hat{h}(r,t) \to \hat{h}[r(1 + A\xi\, e^{im\theta}), t]$.

More details of the growth of the instability are shown in figure 8, which displays the global measures of the perturbation, $\int h'(r,t)r\,dr$ and $\int \Theta'(r,t)r\,dr$, for $m = 3$, 4 and 5. After an initial transient (roughly given by the time needed to form the cooling front), the instability grows approximately exponentially. This motivates the

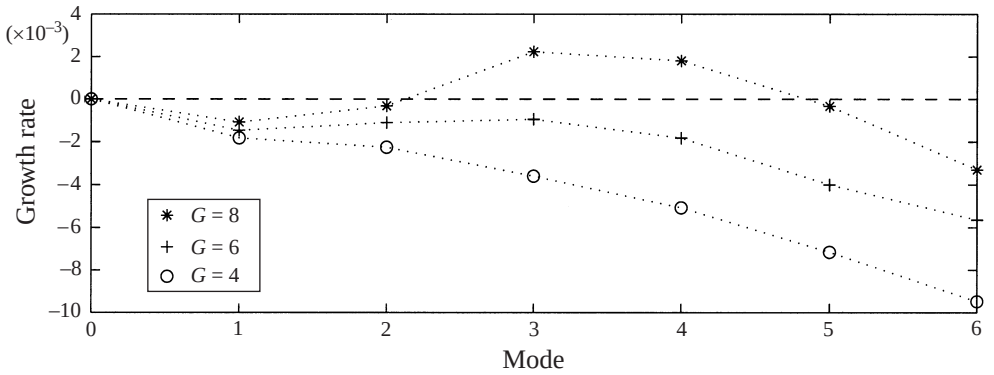

FIGURE 9. The growth rates as defined by (6.6).

definition of a growth rate,

$$\eta = \frac{1}{\Pi} \int_0^{\Pi} \mathrm{d}t \int_0^{r_\infty} \Theta'(r,t) r \, \mathrm{d}r, \tag{6.6}$$

where Π is the length of the computation.

Growth rates for $G = 4, 6$ and 8 are shown in figure 9 for $m = 0, \ldots, 6$. For $G = 8$, the modes with $m = 3$ and 4 are unstable, but the dome with $G = 6$ is stable. Hence there is a critical value for G (just above 6) for instability. Moreover, near onset, $m = 3$ is the preferred mode. Note that the axisymmetrical mode, $m = 0$, has zero growth rate. This is because axisymmetrical perturbations cannot capitalize on the instability mechanism. Also, an $m = 0$ perturbation corresponds to a shift of the equilibrium state to another axisymmetric dome that expands at a similar rate. Hence the mode will neither grow nor decay.

Because the critical value of G is relatively large, and much bigger than what we expect for clay–wax slurries (see table 3), it is unlikely that the non-axisymmetric instability can explain the formation of structure in Griffiths & Fink's laboratory domes. This is consistent with Griffiths & Fink's conclusions that their non-axisymmetric morphology is caused by solidification. Estimates of G are much larger for both lava and syrup (table 3). Hence, the instability may be of geological importance and relevant to the patterns seen in the experiments conducted by Wylie *et al.* (1999). However, there are some problems with the thin-layer theory in these contexts, as discussed next.

7. The limit of small κ

7.1. *Surface thermal boundary layers*

So far, we have described solutions to the thin-layer equations, but have not attempted to compare the results with either real lava or experimental slurries. There is one important aspect of these applications that makes such a comparison especially difficult: as indicated in table 3, for both the lava and slurry the dimensionless diffusion coefficient (inverse Péclet number) κ is small; $\epsilon > \kappa$. But the asymptotic expansion assumes that $\kappa \sim O(1)$ and $\epsilon \ll 1$. Similar theoretical problems plague models of glaciers (Hutter 1983).

A more suitable asymptotic scaling is to take $\kappa = \epsilon^N \tilde{\kappa}$, with $N \approx 5$ for silicic

lava ($\kappa \sim 10^{-5} \sim \epsilon^5$), $N \approx 2$ for basaltic lava and corn syrup ($\kappa \sim 10^{-6} \sim \epsilon^2$ and $\kappa \sim 10^{-2} \sim \epsilon^2$, respectively), and $N \approx 1$ for clay–wax slurries ($\kappa \sim 10^{-3} \sim \epsilon^1$). The dimensionless heat equation then becomes

$$\Theta_t + u\Theta_r + w\Theta_z - \frac{1}{r}\epsilon^N \tilde{\kappa}\partial_r(r\Theta_r) = \epsilon^{N-2}\tilde{\kappa}\Theta_{zz} \tag{7.1}$$

(ignoring frictional heating and non-axisymmetry).

The key physical assumption that underlies the asymptotic theory developed in the earlier sections is that thermal diffusion acts sufficiently quickly to create a dome that is isothermal in the vertical. In the terminology of lava modellers, this is the 'thermally mixed' case, and is often assumed without justification. But to reach such a state, the right-hand side of (7.1) must be the dominant term in the equation. This is guaranteed if $N < 2$, which may be true for wax and clay–wax slurries (but see § 3.1). In other words, although κ is small, the important physical parameter in the heat equation is κ/ϵ^2, which remains large. Physically, this signifies that thermal diffusion proceeds sufficiently quickly to smooth the vertical thermal structure, and justifies the asymptotic theory. In fact, if $N = 1$, one can reformulate the scalings of the expansion to suit this particular case; the only difference in the outcome is a redefinition of the parameters and the disappearance of horizontal diffusion from the heat equation. We have preferred to stay with $N = 0$ in the main discussion because this distinguished limit retains as much of the physics as possible within the confines of a simple thin-layer theory.

However, for silicic lava (with $N > 2$), to leading order, the heat equation becomes

$$\Theta_t + u\Theta_r + w\Theta_z = 0, \tag{7.2}$$

which indicates that fluid advection dominates the thermal evolution. (According to the estimates in table 3, basaltic lava and corn syrup fall midway between the two extremes; in this case one obtains a diffusion–advection equation at leading order). The relevant solution is $\Theta = 1$; fluid expands at the eruption temperature and does not cool. However, heat is still lost from the surface and so a superficial cooling layer develops in which strong temperature gradients appear. This thermal boundary layer extends over a region of size $\zeta = \epsilon^{1-N/2}(h - z)$, wherein we may rewrite the heat equation in the form

$$\Theta_t + u_s\Theta_r + w_{sz}\zeta\Theta_\zeta \sim \tilde{\kappa}\Theta_{\zeta\zeta}, \tag{7.3}$$

where the subscript s indicates the value at $z = h(r, t)$, and $w_{sz}(r, t) \equiv [w_z(r, z, t)]_{z=h}$. This equation models the diffusive advance of the thermal boundary layer into the dome interior.

For viscoplastic domes, provided the boundary layer remains inside the pseudo-plug, thermal effects have no influence on the spreading dynamics because there is little shear inside this region and therefore negligible viscous stress. This leads to the conclusion that a viscoplastic dome will initially expand isothermally at the extrusion temperature. In other words, the pseudo-plug 'shields' the dome from effects of cooling. Shielding fails when the thermal boundary layer finally advances into the yielded region beneath the pseudo-plug. But, this happens on a long, diffusive time scale and will not be important in many situations. The only region which can be seriously affected is near the periphery of the dome, where $h \to 0$ and most time has elapsed.

Because the thermal boundary layer adds vertical structure that is not taken into account, thin-layer theory is of questionable significance for lava. Nevertheless, cooling

is only significant near the dome's edge where $h \to 0$, and there is a crude analogy between the effect of the advancing boundary layer and the simple Newton cooling term, $-\alpha\Theta/h$. However, the thin-layer theory also predicts that, in the limit $\kappa \to 0$ with α finite, the dome always cools. But, with $\kappa \to 0$, the thermal boundary layer never migrates into the fluid interior. In other words, the cooling law is not diffusion-limited in the theory. To remedy this inconsistency one can resort to Galerkin-style techniques to build a diffusion-limited cooling rate into the thin-layer theory. The result replaces the term α with the quantity

$$\tilde{\alpha} \sim \frac{4\epsilon^4\alpha^2}{\pi^2\kappa}\left[\left(1+\frac{\pi^2\kappa}{4\alpha\epsilon^2 h}\right)^{1/2}-1\right]^2, \tag{7.4}$$

which predicts the correct limits as $\epsilon \to 0$ or $\kappa \to 0$ of the cooling rate of the least quickly decaying vertical thermal mode.

However, fundamentally there is a difficulty here that our simple thin-layer theory does not address. We must await the development of a theory that properly builds in the vertical thermal structure. Until then, we hope that our model provides a crude first approximation for building thermal effects into dome models.

8. Concluding remarks

A main goal in the study of lava flows is to infer the conditions under which the lava was extruded, given the morphology of the flow. In their geometrical simplicity, domes provide the first test of theories that attempt to make this inference. Although we are still setting the stage in this and our previous work, our intention is to establish a theoretical foundation upon which to study the issue.

Our approach here has been to use asymptotic expansions to derive a reduced model that avoids the complications of the full problem, but incorporates the essential physics and is still straightforward to solve. The procedure is much like conventional lubrication theory, but novel in that we include yield stresses, shear thinning, temperature-dependent rheology and whatever surface cooling law is appropriate. Moreover, we know of no previous studies that approach the fingering instability problem in the fashion of § 6. That approach was forced upon us because of the inhomogeneous and time-dependent structure of the background state, a complication that does not appear in other fingering problems.

A significant drawback of the thin-layer model derived here is that it is probably a crude approximation for lava and some laboratory analogues: thermal diffusion proceeds too slowly in these fluids to allow us to simplify the heat equation as in § 4. Although this detracts from the general applicability of the theory, our motivation is not entirely one of rigorous asymptotics. Rather, our aim is to derive a useful reduced model of the dome, irrespective of the precise physical conditions in any experiment or geophysical setting. Indeed, the asymptotic scalings comprise a *distinguished limit* of the parameters of the problem. Typically, asymptotic theories derived in a distinguished limit have the disadvantage that they have limited ranges of validity and may not be asymptotic over the parameter range of interest. However, these reduced models contain much of the physics and, in a cruder sense, capture the essence of the full problem. For this reason, we hope the thin-layer equations will provide a useful tool for lava-dome modellers.

By way of illustration, we mention some implications for dimensional analysis. To date, such analysis has been the main theoretical approach to the modelling of

lava domes. But its suitability must be judged by comparison with a more detailed mathematical model, such as the thin-layer theory (at least in cases without thermal boundary layers). Indeed, our thin-layer model verifies the predictions of dimensional analysis in some asymptotic limits (see paper I). However, in paper I we also found that if the dome is not dominated by one particular force balance, the evolution need not follow any of the scaling laws. Moreover, dimensional arguments also predict cross-overs between regimes in which different force balances prevail; we saw little evidence for such transitions in our earlier isothermal computations and experiments. On the other hand, transitions occur in the dominant force balance in non-isothermal domes as a result of cooling. Overall, it seems that dimensional scaling may be misleading without the added foundation of a detailed mathematical model.

Of course, there is much yet missing from the model. An essential next step is to model the boundary-layer structure of the temperature field. Also, we have ignored completely the phase change associated with solidification. In fact, the fluid first solidifies and creates a crust in the surface cooling layer. To model the phase change and the resulting structure of the dome, we need more physics. But that physics is intimately tied to the fluid rheology, which enriches our problem over other fluid solidification problems (e.g. Worster 1997). In analogy with those problems, we anticipate that solidification first produces a 'mushy zone' containing a mixture of fluid and solid (Hills, Loper & Roberts 1982). This zone buffers the molten interior from the solid crust that subsequently forms at the surface, creating a layered structure in the superficial regions of the dome (Neri 1998). The crust can also directly affect the dynamics by contributing additional forces. For example, if the crust forms a solid shell, it may exert a tensile restraining force (Iverson 1990). But if it has a very fractured composition, it may act more like a viscous fluid 'skin' (Scriven 1960).

A further complication is that the crust may become thickest near the dome's edge. In fact, a solid 'talus' typically forms at the rim of a lava dome, composed of solidified material and debris. The expanding dome must push this material ahead of itself, or ride over it, providing extra resistance to the flow. In modelling the talus we would have to deal directly with the contact ring at the edge of the fluid dome. Here, the asymptotic theory formally breaks down, a problem that we have avoided by taking initial conditions in which fluid was present everywhere. But we could consider this ring in more detail, much as has been done in a variety of studies of spreading of liquid drops (Ehrhard & Davis 1991).

Finally, although we have found that domes can suffer non-axisymmetrical instability, we have not given a systematic theoretical study. This is partly because the results do not offer a convincing explanation for the morphology of laboratory slurries; we must await the inclusion of solidification before attempting to rationalize Griffiths & Fink's observations. And for lava, although the parameter values suggest that the instability may operate, our model has no surface cooling layer. In addition, there are mathematical problems with the Eulerian computational scheme because the perturbations diverge at the dome's periphery. We can correct this feature by adopting a Lagrangian description of the fluid (and again dealing with the dynamics of the contact ring), or by considering nonlinear perturbations. We leave both advances for the future.

The financial support of an EPSRC Advanced Fellowship is gratefully acknowledged by R. V. C. N. J. B. thanks the I.S.I. Foundation, Torino, & Imperial College, London (supported by EPSRC Grant GR/M50409) for hospitality during part of this work, and the Nuffield Foundation for an equipment grant.

REFERENCES

Annis, M. R. 1967 High temperature flow properties of water-based drilling fluids. *J. Petrol. Technol.* **19**, 1074–1080.

Aral, B. K. & Kalyon, D. M. 1984 Effects of temperature and surface roughness on time-dependent development of wall slip in steady torsional flow of concentrated suspensions. *J. Rheology* **38**, 957–972.

Balmforth, N. J., Burbidge, A. S., Craster, R. V., Salzig, J. & Shen, A. 1999 Visco-plastic models of isothermal lava domes. *J. Fluid Mech.* **403**, 37–65 (referred to herein as paper I).

Balmforth, N. J. & Craster, R. V. 1999 A consistent thin-layer theory for Bingham fluids. *J. Non-Newtonian Fluid Mech.* **84**, 65–81.

Blake, S. 1990 Viscoplastic models of lava domes. In *Lava Flows and Domes: Emplacement Mechanisms and Hazard Implications* (ed. J. H. Fink), pp. 88–128. IAVCEI Proc. Volcanology, vol. 2, Springer.

Briscoe, B. J., Luckham, P. F. & Ren, S. R. 1994 The properties of drilling muds at high pressures and high temperatures. *Phil. Trans. R. Soc. Lond.* A **348**, 179–207.

Ehrhard, P. 1993 Experiments on isothermal and non-isothermal spreading. *J. Fluid Mech.* **257**, 463–483.

Ehrhard, P. & Davis, S. H. 1991 Non-isothermal spreading of liquid drops on horizontal plates. *J. Fluid Mech.* **220**, 365–388.

Fink, J. H. & Griffiths, R. W. 1990 Radial spreading of viscous-gravity currents with solidifying crust. *J. Fluid Mech.* **221**, 485–510.

Fink, J. H. & Griffiths, R. W. 1992 A laboratory study of the surface morphology of lava flows extruded from point and line sources. *J. Volcan. Geotherm. Res.* **54**, 19–32.

Fink, J. H. & Griffiths, R. W. 1998 Morphology, eruption rates and rheology of lava domes: insights from laboratory models. *J. Geophys. Res.* **103**, 527–545.

Griffiths, R. W. & Fink, J. H. 1993 Effects of surface cooling on the spreading of lava flows and domes. *J. Fluid Mech.* **252**, 667–702.

Griffiths, R. W. & Fink, J. H. 1997 Solidifying Bingham extrusions: A model for the growth of silicic lava domes. *J. Fluid Mech.* **347**, 13–36.

Hills, R. N., Loper, D. E. & Roberts, P. H. 1982 A thermodynamically consistent model of a mushy zone. *Q. J. Mech. Appl. Maths* **36**, 505–539.

Huppert, H. E., Shepherd, J. B., Sigardsson, H. & Sparks, R. S. J. 1982 On lava dome growth. *J. Volcan. Geotherm. Res.* **14**, 199–222.

Hutter, K. 1983 *Theoretical Glaciology*. D. Reidel.

Iverson, R. M. 1990 Lava domes modeled as brittle shells that enclose pressurized magma. In *Lava Flows and Domes: Emplacement Mechanisms and Hazard Implications* (ed. J. H. Fink), pp. 47–69. IAVCEI Proc. Volcanology, vol. 2, Springer.

Jensen, O. E. & Grotberg, J. B. 1993 The spreading of heat or soluble surfactant along a thin film. *Phys. Fluids* A **5**, 58–68.

King, J. R., Riley, D. S. & Sansom, A. 2000 Gravity currents with temperature-dependent viscosity. *Comp. Assist. Mech. Eng. Sci.*, to appear.

McBirney, A. R. & Murase, T. 1984 Rheological properties of magmas. *Ann. Rev. Earth Planet. Sci.* **12**, 337–357.

Neri, A. 1998 A local heat transfer analysis of lava cooling in the atmosphere: application to thermal diffusion-dominated lava flows. *J. Volcan. Geotherm. Res.* **81**, 215–243.

Patterson, L. 1981 Radial fingering in a Hele-Shaw cell. *J. Fluid Mech.* **113**, 513–529.

Pearson, J. R. A. 1977 Variable-viscosity flows in channels with high heat generation. *J. Fluid Mech.* **83**, 191–206.

Pinkerton, H. & Norton, G. 1995 Rheological properties of basaltic lavas at sub-liquidus temperatures: laboratory and field measurements on lavas from Mount Etna. *J. Volcan. Geotherm. Res.* **68**, 307–323.

Pinkerton, H. & Stevenson, R. J. 1992 Methods of determining the rheological properties of magmas at sub-liquidus temperatures. *J. Volcan. Geotherm. Res.* **53**, 47–66.

Scriven, L. E. 1960 Dynamics of a fluid interface: Equation of motion for Newtonian surface fluids. *Chem. Engng Sci.* **12**, 98–108.

Shaw, H. R. 1969 Rheology of basalt in the melting range. *J. Petrol.* **10**, 510–535.

Spera, F. J., Borgia, A. & Strimple, J. 1988 Rheology of melts and magmatic suspensions 1. Design and calibration of concentric cylinder viscometer with application to rhyolitic magma. *J. Geophys. Res.* **93**, 10273–10294.

Stasiuk, M. V., Jaupart, C. & Sparks, R. S. J. 1993 Influence of cooling on lava-flow dynamics. *Geology* **21**, 335–338.

Tanner, R. I. 1985 *Engineering Rheology*. Clarendon.

Whitehead, J. A. & Helfrich, K. R. 1991 Instability of flow with temperature-dependent viscosity – a model of magma dynamics. *J. Geophys. Res.* **96**, 4145–4155.

Worster, M. G. 1997 Convection in mushy layers. *Ann. Rev. Fluid Mech.* **29**, 91–122.

Wylie, J. J., Helfrich, K. R., Dade, B., Lister, J. R. & Salzig, J. F. 1999 Flow localization in fissure eruptions. *Bull. Volcan.* **60**, 432–440.